Arab J Sci Eng (2013) 38:953–970
DOI 10.1007/s13369-012-0374-3

RESEARCH ARTICLE - MECHANICAL ENGINEERING

The Diagnostics of Abrasive Tools After Internal Cylindrical Grinding of Hard-to-Cut Materials by Means of a Laser Technique Using Imaging and Analysis of Scattered Light

W. Kapłonek · K. Nadolny

Received: 15 November 2010 / Accepted: 5 May 2011 / Published online: 11 October 2012

Abstract The formation of smears on the grinding wheel active surface is one of most undesirable phenomena during abrasive machining. Intensive growth of such smears leads to a decrease in the machining capacity of the grinding wheel, which, in turn increases the grinding power and the effects of friction upon the process, reducing efficiency. What is very important in this context is the possibility to inspect the condition of the grinding wheel active surface during the grinding process in order to detect the excessive growth of smears. Such an inspection can be carried out by automatic machine vision systems, or systems using optical measuring methods (especially those from a group of light scattering methods). In the paper is presented and discussed a proposal for optical inspection using laser scatterometry, as well as image processing and analysis techniques. It involves the acquisition of an image of scattered light during the illumination of tested surfaces by a laser light (wavelength $\lambda = 635$ nm). The analysis of such an image can enable the procurement of the values of geometric and photometric parameters, which then be correlated with, for example, the selected parameters of surface roughness obtained by other techniques. Experimental investigations were carried out on grinding wheel active surfaces after internal cylindrical grinding of hard-to-cut materials. The discussed methods were confirmed to be useful, which could be an interesting alternative to solving the important problem of diagnostics of abrasive tools in machining processes.

W. Kapłonek · K. Nadolny (✉)
Department of Mechanical Engineering, Koszalin University of Technology, Racławicka 15-17, 75-620 Koszalin, Poland
e-mail: krzysztof.nadolny@tu.koszalin.pl

Keywords Diagnostics of abrasive tools · Internal cylindrical grinding · Hard-to-cut materials · Laser scatterometry · Image processing and analysis

الخلاصة

إن تشكيل المسحات على السطح النشط لعجلة الطحن هي واحدة من أكثر الظواهر غير المرغوب فيها خلال تشكيل الكشط . ويؤدي النمو المكثف لهذه المسحات إلى انخفاض في القدرة على التشكل لعجلات الطحن الذي يزيد بدورة من قدرة الطحن والآثار المترتبة على العملية ، وتعليل الكفاءة . ماهو مهم جدا في هذه السياق؟ هو إمكانية فحص حالة السطح الفعال لعجلات الطحن خلال عملية الطحن من أجل الكشف عن النمو المفرط للمسحات. ويمكن تنفيذ مثل هذا الفحص بوساطة أنظمة الرؤية للآلة الأوتوماتيكية والأنظمة التي تستخدم طرق القياس البصرية (لاسيما طرق تشتت الضوء).

في هذه الورقة هناك عرض ومناقشة مقترح للفحص البصري مع استعمال علم تشتت الليزر، وكذلك تقنيات معالجة الصورة والتحليل. وهي تنطوي على إكتساب صورة الضوء المشتت خلال إضاءة الأسطح التي تم اختبارها بوساطة ضوء الليزر. (الطول الموجي $\lambda = 635$ نانومتر). إن تحليل مثل هذه الصور يمكّن من شراء قيم المعاملات الهندسية والضوئية الذي يمكن ربطها بعد ذلك على سبيل المثال بالمعاملات المختارة لخشونة السطح التي تم الحصول عليها بوساطة تقنيات أخرى . ثم إجراء فحوصات مختبرية على الأسطح النشطة لعجلة الطحن بعد الطحن الأسطواني الداخلي للمواد الصلبة ـ للقطع. وقد تم التأكد من الطرق التي تمت مناقشتها وكانت مفيدة ويمكن أن تكون بديلا مهما لحل مشكلة مهمة التشخيص لأدوات الكشط في عملية التصنيع.

Abbreviations

ASTM	American Society for Testing and Materials
AFNOR	Association Française de Normalisation
ROI	Region of interest
BS	British standard
GSS	Geometrical structure of surface
HT	Heat treatment

SAE	Society of Automotive Engineers
UNS	Unified numbering system
a_e	Working engagement (mm)
A_n	Area (of the bright regions of an image of scattered light) (pixel)
b_w	Workpiece breadth (mm)
d_s	Grinding wheel diameter (mm)
d_w	Workpiece diameter (mm)
D	Grinding wheel outside diameter (mm)
H	Grinding wheel inside diameter (mm)
I_Σ	Integrated optical density (of the bright regions of an image of scattered light) (a.u.)
$\boldsymbol{n}$	Normal to nominal surface
n_s	Grinding wheel rotational frequency (rpm)
n_w	Workpiece rotational frequency (rpm)
l	Tracing length (mm)
l_{max}	Max. traverse (mm)
Q_c	Coolant flow rate (l/min)
Q_w	Material removal rate (mm^3/s)
r	(Tip) radius (μm)
Sa	Arithmetic mean height (μm)
Sdr	Developed interfacial area ratio (%)
Sk	Kernel roughness depth (roughness depth of the core) (μm)
St	Total height of the surface (μm)
t_{exp}	Exposure time (s)
t	Grinding time (s)
T	Grinding wheel total height in axial direction (mm)
Ua	Accelerating voltage (kV)
v_{fr}	Radial table feed speed (mm/s)
v_s	Grinding wheel peripheral speed (m/s)
v_w	Workpiece peripheral speed (m/s)
V	Tracing speed (mm/s)
V_w	Material removal (mm^3)
θ_i	Angle of incidence of light onto the surface (°)
θ_s	Angle of reflection of light at a point in surface (°)
λ	Wavelength (nm)
σ	Standard deviation

1 Introduction

The lengthy contact between grinding wheel and workpiece, which takes place in the internal cylindrical grinding processes [1–5], presents difficulties for the effective insertion of cooling fluids into the grinding zone. Also chips and other grinding products are not properly removed from the contact zone. One result of these undesirable conditions is the proliferation of the smearing phenomenon upon the grinding wheel active surfaces. This phenomenon is especially intense in the event of grinding hard-to-cut materials [6–10], such as new variations of alloy steels and alloys on the basis of nickel, cobalt or titanium (INCONEL®, INCOLOY®, NIMONIC®, HASTELLOY® etc.), which are very ductile, resistant, hard and have small thermal conductivity.

Of great significance to the internal cylindrical grinding of hard-to-cut materials are the possibilities for monitoring and measuring the degree to which smearing occurs upon the grinding wheel active surface. The precise determining of the moment when regeneration is necessary is crucial because it can impact upon the workpiece surface quality and the durability of the grinding wheel. In extreme cases the rapid growth of smears can increase the friction participation and accelerate an excessive rise in temperature. Finally, grinding defects [6,11] could occur upon the workpiece surface, or increasing temperature stresses could result in disruption to the grinding wheel itself.

The assessment of the degree to which smearing effects the grinding wheel active surface can be carried out using various measuring methods, but most often official methods are utilized. From the many groups of optical methods, which can be used in this type of assessment, the most important are methods based on light scattering phenomenon. These methods are generally known as scatterometry. The many significant advantages of scatterometry (non-contact method of measurement, short-time of measurement, high sensitivity and accuracy) can be a good alternative to other methods (pneumatic, ultrasonic). The possibility of integrating this method with image processing and analysis techniques may, additionally, lead to the acquirement of an effective measuring instrument, designed for diagnostics of abrasive tools.

2 Machining Process and Measurement Method

2.1 Internal Cylindrical Plunge Grinding

Grinding wheels with the following technical designations underwent examination, 1−35×20×10-SG/F46 K7VTO, with which grinding tests of hard-to-cut materials were carried out in the process of plunge peripheral grinding of internal cylindrical surfaces [1,2]. The method consisted in carrying out a short grinding test, lasting approximately 3 s on a properly shaped grinding wheel, in the plunge grinding kinematics. The test was carried out without the finish grinding and sparking out stages. The grinding wheel carried out its working movement with the given feed speed v_{fr}, after which it was immediately moved away from the processed material. What was characteristic of the method used was the modification of the geometry of the grinding wheel, which consisted of forming a few zones of various diameters (Fig. 1a) on its active surface in the dressing process.

When performing tests using grinding wheels with various diameters, it must be prepared in such a way so as to obtain an even division of the total height of the grinding wheel in the axial direction T to particular working zones

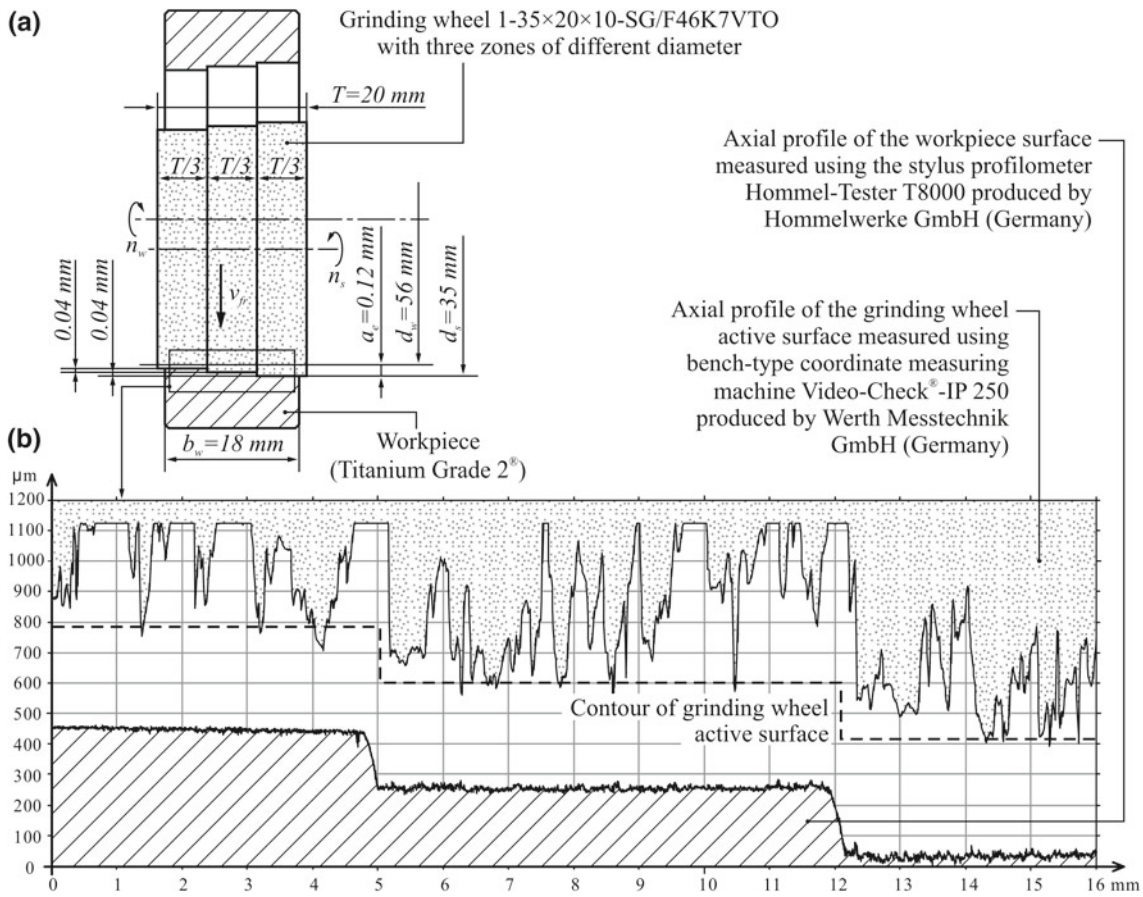

Fig. 1 Schematic diagram of grinding process (**a**) as well as the setting-up of measured axial profiles of the grinding wheel and workpiece after plunge grinding using a grinding wheel with zones of various diameter (**b**)

(Fig. 1a). The methodology used also assumed that the total working engagement a_e is divided equally amongst subsequent steps of the grinding wheel. Such plunge grinding, results in representing the shape of the grinding wheel on the workpiece (Fig. 1b). Quick backwards movement and omission of sparking out results in an abrupt interruption of the grinding process. Special shaping of the macrogeometry of the grinding wheel [3] makes particular parts of its active surface work at different times and remove different material volumes. In consequence, in particular areas of the grinding wheel active surface, the processes of wearing off of the abrasive grains [11], chip formation and smearing the intergranular free spaces take place with various intensity and can take different forms.

2.2 Mechanism of the Smear Forming

The phenomenon of smearing the grinding wheel active surface with chips from the machined material and other grinding products (crumbled abrasive grains, bond) takes place as a result of excessive temperature increase in the area of contact of the grinding wheel and the machined material. Quite often such temperature growth is caused by increasing friction forces in the grinding process [6,11]. This is true mainly for machined materials with poor heat conductivity. Smears are formed in areas of contact between the grinding wheel active surface and the workpiece, such as vertexes of the abrasive grains. An example of smearing upon the microvertexes of a SG microcrystalline sintered corundum abrasive grain is presented in Fig. 2.

Under the exceptionally difficult working conditions of the grinding wheel active surface, smears of significant surface area can be formed, which would include both grains and intergranular free spaces (Fig. 3). The reason for their formation is most frequently excessive material removal rate, wearing off of the grinding wheel, as well as too few intergranular free spaces, which do not guarantee effective transportation of the grinding products beyond the processing area and do not provide efficient supply of the cooling liquid to the grinding zone.

This phenomenon can occur with higher intensity in grinding processes, in which the path of contact of the grinding wheel with the material is longer, as in the case of internal cylindrical grinding, for example. What plays a significant

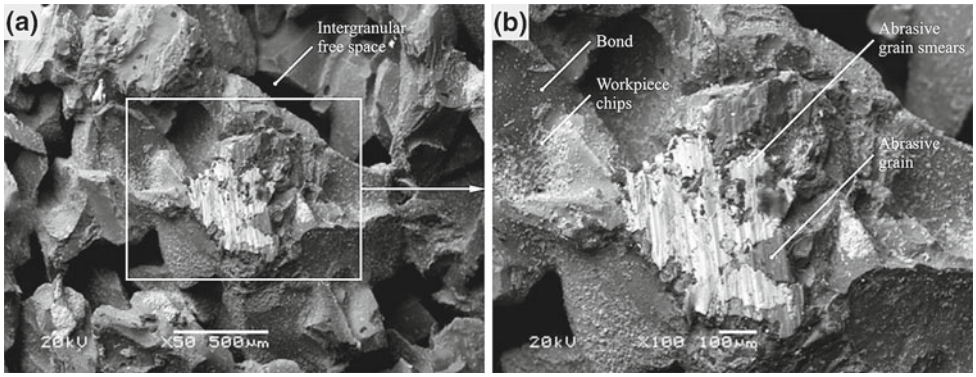

Fig. 2 Micrograph of visible smear of microvertex of a SG microcrystalline sintered corundum abrasive grain obtained by JEOL JSM 5500LV scanning electron microscope produced by JEOL Ltd.: **a** Ua = 20 kV, Mag. ×50, **b** Ua = 20 kV, Mag. ×100

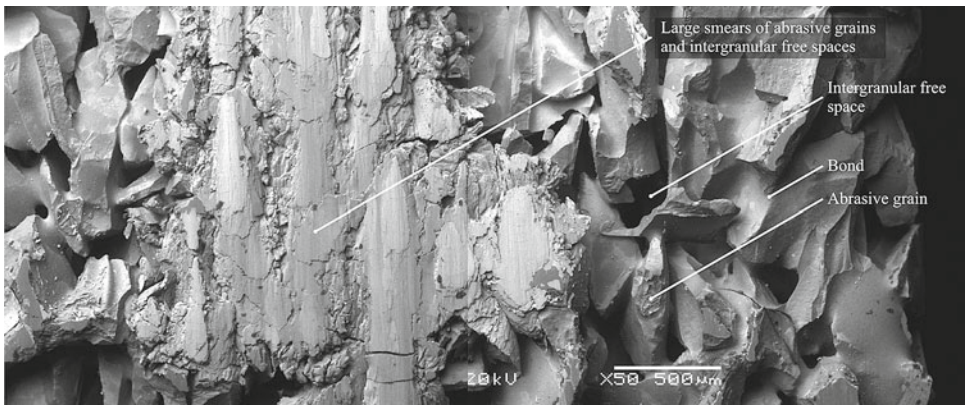

Fig. 3 Micrograph of visible smear of intergranular space of grinding wheel active surface after grinding Titanium Grade 2® obtained by JEOL JSM 5500LV scanning electron microscope produced by JEOL Ltd. (Ua = 20 kV, Mag. ×50)

role in the prevention of smearing on the grinding wheel active surface is the type, outlay and method of application of the cooling liquid.

Smears upon the grinding wheel active surface lead to excessive temperature increase in the area of contact of the grinding wheel with the machined material, which can cause the appearance of grinding defects, such as grinding burns or microfractures of the top layer of the machined surface. The decrease in the number of cutting apexes, caused by the smears, deteriorates the cutting capacity of the grinding wheel and may have an influence on the effectiveness of the machining process, as well as the attainment of surface roughness and dimensional-shaped precision. As the smears cause significant temperature growth, mainly in the grinding wheel, in the case of grinding wheels with ceramic bond to the destruction of the tool, caused by the uneven distribution of the thermal stress in the grinding wheel's mass.

2.3 Light Scattering and Light-Scattering-Based Methods

The surface roughness assessment and detection of surface defects using scattered light is based on the observation of light reflected in a different way from a smooth surface and a rough one. These cases are shown in Fig. 4.

The mathematical description of the above-detailed cases is given in principle light scattering theories—Kirchhoff's diffraction theory and Rayleigh–Rice's perturbation theory. The wide review of these theories was presented in Refs. [12,13]. Many optical measuring methods are based on light scattering phenomenon. The most dynamically developed for many years are the following methods: reflectometry [14], total integrated scattering (TIS) [15], angle-resolved scattering/differential scattering (ARS/DS) [16] and optical Fourier transform (OFT) [17]. These methods often use laser radiation (visible light or infrared ranges from 0.75 to 15 μm) and are thus defined by one general term—laser scatterometry [18–20].

Laser scatterometry allows for the assessment of very small surface irregularities that are distributed over, e.g., precision optical elements [21], silicon wafers [22] and thin films [23]. The height of these irregularities ranges from 0.1 nm to several nanometers. The great advantages of these methods are their high sensitivity, the fact that they offer a non-contact form of measurement, short-time of surface roughness assessment and the possibilities for detection of surface defects.

The measurements which are realized by laser scatterometry often relate to the assessment of machined surfaces made of metal or its alloys, carried out in high-efficiency machining processes such as grinding [24], polishing [25], lapping [26], microfinishing [27]. In this case, the height of irregularities could reach a somewhat higher value, even close to several micrometers. Much less frequently, in the literature, instances can be found which use these methods

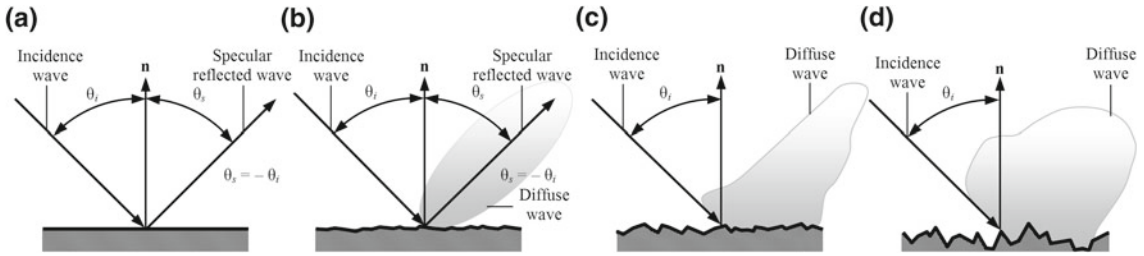

Fig. 4 Reflection of the light from surface: **a** smooth surface, **b** slightly rough surface, **c** moderately rough surface, **d** very rough surface (θ_i—angle of incidence of light onto the surface, θ_s—angle of reflection of light at a point in surface, ***n***—normal to nominal surface)

to assess surfaces made of plastics and ceramics. From this last material abrasive tools are commonly produced. They are difficult to assess by laser scatterometry methods. It depends mainly from constructions of grinding wheels (stochastically packed grains bonded by binder). This highly heterogeneous structure, without visible directivity of machined grooves, is causing the increase of the light scattering phenomenon. It visually manifests in creating on observation plan an irregular shape of an image of scattered light (Fig. 5f). This image is totally different from the images created for typical machined surfaces which are shown in Fig. 5.

To improve the accuracy and efficiency of the assessment of surface roughness and detection of surface defects, laser scatterometry can be supported, in many cases, by image analysis techniques [27]. It concerns both types of measurement, those carried out in static conditions and those carried out in motion [28]. Image analysis, realized by use of specialist software, can present many possibilities to carry out complicated multi-criterion quantitative and qualitative analysis, in manual or automatic mode, measuring the geometrical quantities of elements in image and the visualization of measurement data.

3 Experimental Investigations

The main goals of the experimental investigations were:

1. analysis of the possible use of laser scatterometry, and image processing and analysis techniques, in the optical inspection of the condition of the grinding wheel active surface,
2. development of a correct methodology for the inspection of grinding tool surfaces that have visible smears, using images of scattered light, carry out tests on grinding wheels smeared with various types of hard-to-cut material, characterized by different properties.

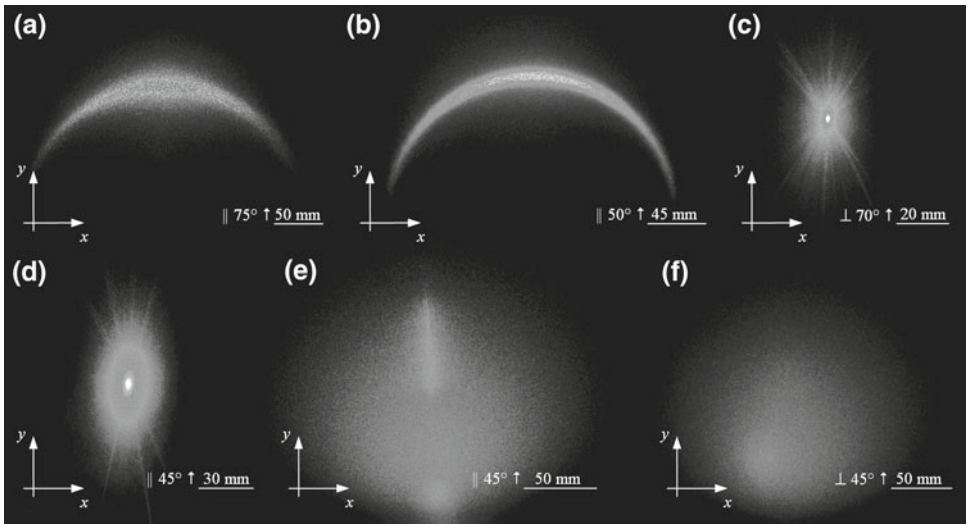

Fig. 5 The comparison of images of scattered light acquired for: **a** ground surface made of EN C45 steel ($Ra = 6.3\,\mu m$), **b** face turned surface made of EN C45 steel ($Ra = 0.84\,\mu m$), **c** polished surface made of EN AW-6082 aluminium ($Ra = 0.05\,\mu m$), **d** polished surface made of EN CW612N brass ($Ra = 0.08\,\mu m$), **e** microfinished surface made of Ertalon® LFX ($Ra = 0,17\,\mu m$), **f** surface of diamond grinding wheel with zone diversified structure $1-35\times20\times10$-SG/F46 K 7 V TO ($Ra > 3\,\mu m$). ∥—tested surface is illuminated by laser light beam when plane of incidence is parallel to axis of sample, ⊥—tested surface is illuminated by laser light beam when plane of incidence is perpendicular to axis of sample, °—angle of incidence of the laser light beam, ↑—measurement is carried out in static condition

Experimental investigations were realized in five steps, which will be fully described in this section.

3.1 Step 1: Abrasive Machining with the Aim of Forming the Smears

The experimental investigations were carried out using three different hard-to-cut materials—Titanium Grade 2®, INCOLOY® alloy 800HT® and INCONEL® alloy 600. A typical 100Cr6 steel was used as a reference material. The characteristics of the tested materials are given in Table 1.

The above-mentioned materials underwent plunge grinding utilizing a grinding wheel with a specifically shaped macrogeometry of the active surface, according to the diagram presented in Fig. 1a. The total working engagement in Zone I was 0.04 mm, in Zone II 0.08 mm and in Zone III 0.12 mm. The machining time resulted from the assumed radial table feed speed $v_{fr} = 0.04$ mm/s and was, respectively, for the subsequent zones: $t_I \approx 1$ s, $t_{II} \approx 2$ s, $t_{III} \approx 3$ s. With such machining parameters, three zones with variable material removal value V_w were obtained and its value fluctuated from 42.22 mm^3 for Zone I, to 126.67 mm^3 in Zone III. The internal cylindrical plunge grinding with purposefully applied high material removal rate ($Q_w \approx 42$ mm$^3/s$) soon led to the appearance of smears on the grinding wheel active surface, which were then measured.

3.2 Step 2: Acquisition of Images of Scattered Light

Acquisition of images of scattered light were carried out by an experimental setup that included a single semi-conductor laser CPS180 produced by Thorlabs, Inc. (Sweden), which emitted a continuously visible light beam (wavelength $\lambda = 635$ nm). The beam was directed at an angle of 45° and illuminated the surface of the grinding wheel, mounted in a specially designed holder, generating a 1-mm diameter spot on it. As a result of light scattering on the tested surface, an image of angular distribution of the scattered light intensity was created in the observation plane. The scattered light was observed on a matt screen with a scale for initial calculations of dimension of the generated image. The acquisition was carried out under static conditions for all of the 3 zones, which selected 14 areas with or without visible smears, when the angle of incidence was parallel to the grinding wheel axis. Each area had a size of 5 × 5 mm. Within each area 25 images of scattered light, for all points, were acquired. During acquisition of the images of scattered light, the surface of the grinding wheel was dry. The methodology of acquisition of the images of scattered light is shown in Fig. 6.

The scattered light images were acquired by digital camera Camedia C-5060WZ produced by Olympus (Japan) and fixed on a tripod. The images were acquired with the following parameters: exposure time $t_{exp} = 1$ s, image resolution 2,592 × 1,944 pixels, sensitivity ISO 400, saving format *.jpg. Figure 7 shows exemplary images of scattered light which were acquired during the experiments. The images were shown in the following order: zone number, area number and number of a single point.

3.3 Step 3: Computer Image Processing and Analysis

In the last stage of the experimental investigations, images of the scattered light underwent analysis using Image-Pro® Plus 5.1.0.20. software produced by Media Cybernetics, Inc. (USA). The analysis included calculating the values of some selected geometric and photometric parameters from the acquired images. The characteristics of these parameters are given in Table 2. Before the actual analysis took place, the images were pre-processed. Their resolution was decreased to size 640 × 480 pixels with the aim of accelerating image

Table 1 The characteristics of the tested hard-to-cut materials and reference material

Sample no.	Material	Material no.	Standard	Chemical composition and percentage of elements (%)
1	Titanium Grade 2®[a]	3.7035	UNS R50400 ASTM B861	C(0.08) + Fe(0.25) + O(0.25 max) + Ni(0.03) + H(0.015 max) + Ti(Balance)
2	INCOLOY® alloy 800HT®[a]	1.4876	UNS N08811 ASTM B407	Ni(30.0–35.0) + Fe(39.5 min) + Cr(19.0–23.0) +C(0.10 max) + Al(0.1–0.60) + Ti(0.15–0.60) +Mn(1.50 max) + Cu(0.75 max) +S(0.015 max) + Si(1.0 max)
3	INCONEL® alloy 600[a]	2.4816	UNS N06600 ASTM B167	Ni + Co(72.0 min) + Cr(14.0–17.0) + Fe(6.0–10.0) +C(0.15 max) + Mn(1.0 max) + S(0.015 max) +Si(0.50 max) + Cu(0.50 max)
4	100Cr6 steel[b]	1.3505	BS 2S135 AFNOR 100C6 SAE 52100	C(0.93–1.05) + Si(0.15–0.35) + Mn(0.25–0.45) +P(0.025) + S(0.015) + Cr(1.35–1.60) + Mo(0.10)

INCOLOY® and INCONEL® are trademarks of Special Metals Corporation (USA)
[a] Material is produced by Special Metals Corporation (USA) and distributed by Bibus Metals (Switzerland)
[b] Material is produced and distributed by Trafileria A. Mauri e Figli (Italy)

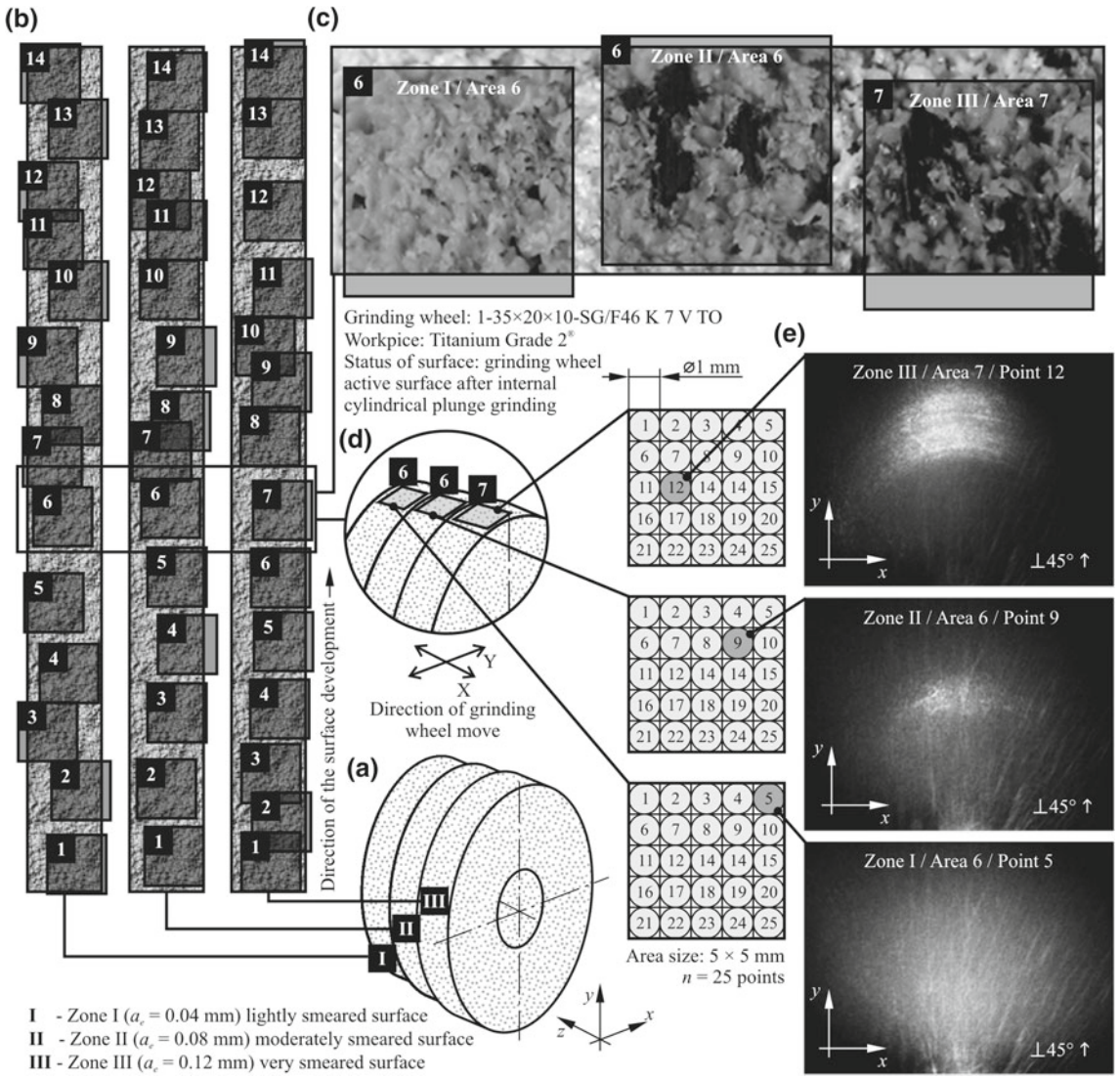

Fig. 6 The methodology for the acquisition of images of scattered light: **a** schematic view of grinding wheel with 3 selected zones, **b** 3 zones of grinding wheel in developed view with 14 selected areas for each zone, **c** macro-graph of fragment of real surface of the grinding wheel with 3 selected areas, **d** selected detail of surfaces with 3 areas (each area was 5 × 5 mm in size and contained 25 points at which we were carrying out acquisition of images of scattered light), **e** corresponding to selected areas images of scattered light obtained for exemplary points 12, 9, 5

analysis; with use of the software, brightness and contrast were corrected and the images were suitably framed. Then the prepared images were analyzed. For this purpose the software segmented particular images to obtain the outlines necessary for calculating the values of geometric parameters, or utilized tonal correction, to improve brightness and contrast, helping to obtain the correct values of the photometric parameters, amongst other things.

Regardless of the method of initial processing of the images, the above-mentioned parameters were obtained using the *Count/Size* function. It enabled the authors to perform the quantity analysis on the basis of the automatic counting of all dark objects in all images of scattered light.

3.4 Step 4: Measurements of Surface Microtopography

The initial assessment of the results obtained with computer image analysis showed the existence of a couple of exceptionally interesting surface images in each of the zones of the tested surfaces. The authors came to the conclusion that these areas should also be analyzed in relation to the value meaning of the chosen surface microtopography parameters, which would correlate with parameters determined from the images of scattered light. For this purpose, two referential methods were used—optical profilometry and stylus profilometry.

The first method connected directly to the machining tool, making it possible to realize the topographical

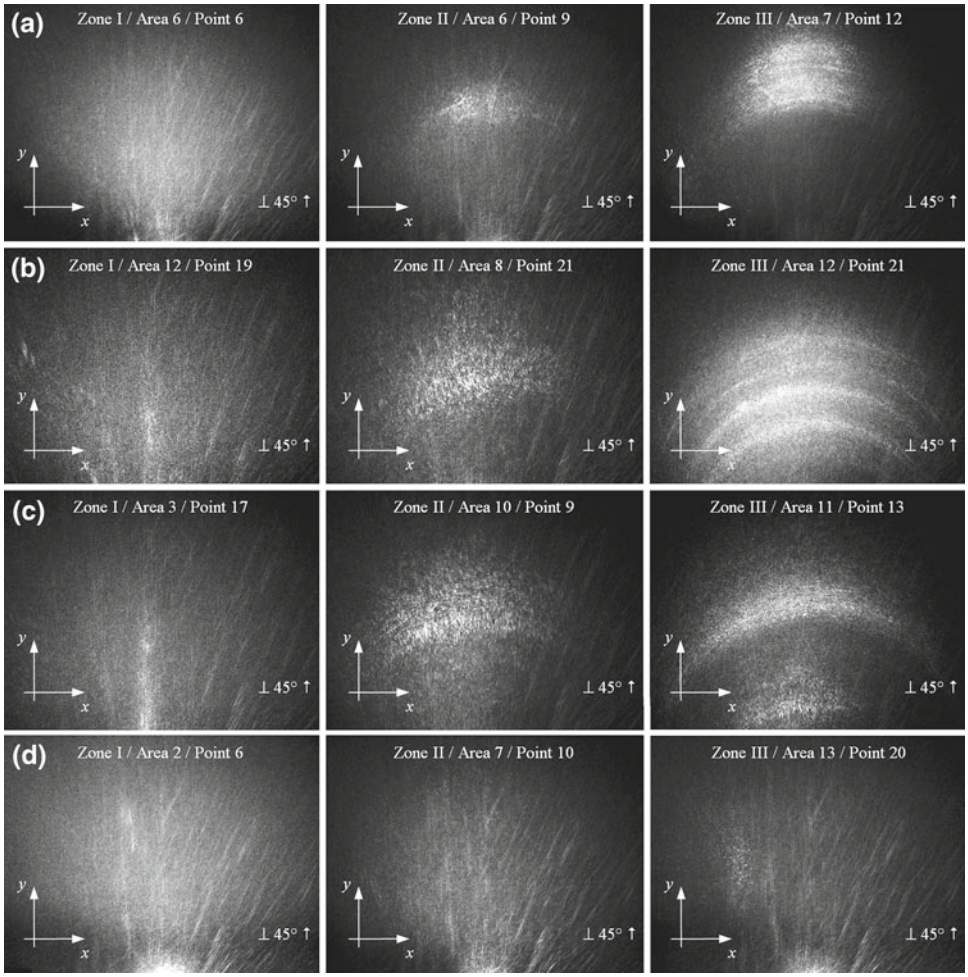

Fig. 7 Exemplary images of scattered light obtained during illumination of surfaces of tested samples by laser beam light (wavelength $\lambda = 635$ nm), when the plane of incidence was parallel to axis of the grinding wheel. Images are presented for a single point in a selected area of one of the three zones each grinding wheel sample was made of: **a** Titanium Grade 2®, **b** INCOLOY® alloy 800HT®, **c** INCONEL® alloy 600, **d** 100Cr6 steel (reference material)

Table 2 The characteristics of calculated parameters from images of scattered light

Group of parameters	Parameter	Designation	Unit	Interpretation
Geometric	Area	An	pixel	Area of each object in image belongs to ROI
	Size (length)	l	pixel	Feret diameter (caliper length) along a major axis of the object
	Size (width)	t	pixel	Feret diameter (caliper length) along a minor axis of object
Photometric	Heterogeneity	SF	a.u.	Fraction of pixels that deviate more than 10 % from the average intensity of the object
	Integrated optical density (IOD)	I_Σ	a.u.	Average intensity/density of each object. This value is expressed in terms of the current intensity/density mode and calibration
	Margination	M	a.u.	Distribution of intensity between the center of an object and the edge of the object

measurements of the tested grinding wheels active surface. During these measurements an optical profilometer Talyscan 150, produced by Taylor Hobson Ltd. (UK), was used. This non contact scanning instrument was equipped with a laser measuring head with vertical resolution 1 μm. All micro-topographies were registered using laser triangulation for a 19.0×10.0 mm surface area. The measurement was made in 201 passes with a sampling step 50 μm in a double-pass mode, i.e., registration of data took place in both directions on the measured surface. In a single pass approximately 1,900 points were registered with the tracing speed $V = 5.5$ mm/s. The Talyscan 150 was also equipped with dedicated software—Talyscan 1.0. and TalyMap Universal 3.1.0. using Mountain Technology™ provided by Digital-Surf (France). The first of these programs was used for the control of measuring elements and for setting conditions for

measurements. The second was mainly used to aid the analysis and visualization of the obtained measurement data.

The second method, connected with the machined object, made it possible to obtain parameters for the microtopography of the surface of cylindrical elements made from hard-to-cut materials, which had underwent plunge grinding. In this case, the Hommel-Tester T8000 produced by Hommelwerke GmbH (Germany) was used. The stylus profilometer, was equipped with a TKL100 pick-up with diamond stylus tip (tip radius $r = 2.5\,\mu\text{m}$). Hommel-Tester T8000 used traverse unit Waveline™ 60 Basic (tracing length $l = 60$ mm), which was mounted on measuring column Wavelift™ 400 M (max. traverse $l_{\max} = 400$ mm). The column was mounted on a granite plate Wavesystem™ 780. In the plate was a groove for mounting a motorized positioning stage (Y-Positioner) equipped with a stepper motor, intended to carry out precise movements in the y-axis. All microtopographies in this case were registered for a 17.0×5.0 mm surface area. The measurement was made in 251 passes with a sampling step $20\,\mu\text{m}$ in a single-pass mode, i.e., registration of data took place only in one direction on the measured surface. In a single pass approximately 9,581 points were registered with the tracing speed $V = 0.15\,\text{mm/s}$. The stylus profilometer used a similar software package as an optical profilometer. Turbo Roughness for Windows 3.1 was used for the control of measuring elements as well as for setting conditions for measurements. For analysis and visualization of the obtained measurement data HommelMap Basic 3.1.0, using Mountain Technology™ provided by DigitalSurf (France), was used. During both type of measurements (stylus and optical) the surface of machining tool and the surface machined object was dry.

From a number of determined geometrical structure of surface (GSS) parameters only those which showed the highest sensitivity to changes in the surface features, caused by smears, were used. These were the four parameters: arithmetic mean high *Sa*, total height of the surface *St*, kernel roughness depth *Sk* and developed interfacial area ratio *Sdr*. The characteristics of these parameters are given in Table 3.

3.5 Step 5: Acquisition of Microscopic Images

The last step of the investigation was the acquisition of the micrography of selected areas of the grinding wheel active surface, with and without visible smears. In this case a scanning electron microscope JSM5500LV, produced by JEOL Ltd. (Japan), was used. Samples were placed in the microscope chamber without any special preparation. The images were obtained with 50×, 100×, 500× magnification with an accelerating voltage of 15–20 kV.

4 Results and Discussion

As a result of a number of operations described in Sect. 3, very extensive research material was obtained. It comprised results obtained from:

1. computer analysis of the images of scattered light,
2. optical measurements of selected areas of the grinding wheel active surface,
3. stylus measurements of selected areas of the grinding wheel active surface,
4. visual analysis of the micrographs.

All of the above will be discussed in detail in this section.

The computer image analysis was carried out in the Image-Pro® Plus 5.1.0.20 environment and consisted of defining the value of the set of geometrical and photometrical parameters given in Table 3. The authors notice that the set of the

Table 3 The characteristics of calculated parameters of surface microtopography

Group of parameters	Parameter[a]	Designation	Unit	Interpretation
Amplitude	Arithmetic mean height	$Sa^{b/c}$	μm	Mean of the absolute values of the profile heights measured from a mean line averaged over the profile
	Total height of the surface	St^{c}	μm	Height between the highest peak and the deepest hole. This parameter is supplied in conformity with the 2D parameters
Functional	Kernel roughness depth (roughness depth of the core)	$Sk^{b/c}$	μm	*Sk* is the efficient roughness of the profile. It is the height of the roughness profile, without taking into account the elevated peaks or the very deep holes
Hybrid	Developed interfacial area ratio	$Sdr^{b/c}$	%	The developed surface indicates the complexity of the surface thanks to the comparison of the curvilinear surface and the support surface. A completely flat surface will have a *Sdr* near 0 %. A complex surface will have a *Sdr* of some percent

[a] All parameters are included in the EUR 15178 EN report [29]
[b] Parameters calculated for the abrasive tool surface
[c] Parameters calculated for the workpiece surface

proposed parameters does not fully reflect the characteristics of the surfaces under investigation. The parameters have successfully been used in assessing the surfaces made from plastics, metals and metal alloys. However, bearing in mind the totally different characteristics of the abrasive tool's surface (especially its considerable heterogeneity), it was necessary to find in both of the groups those parameters which would make it possible to find out more about the surface being assessed. After a detailed analysis, one parameter of both the groups was proposed.

The parameters proposed were:

1. geometrical parameter: A_n—area (of the bright regions of an image of scattered light),
2. photometrical parameter: I_Σ—integrated optical density—IOD (of the bright regions of an image of scattered light).

The above-mentioned parameters turned out to be key for computer analysis of the images of scattered light and were clear referents for other determined parameters. Due to the above-mentioned reasons, the authors decided to graphically present results of the measurements, using only these two key parameters.

Figure 8 presents the results of computer image analysis—calculated average values of areas of the bright regions of an image of scattered light for the sample number. In each column of the graphs, the values of standard deviation σ are also indicated. Additionally, the average values of the area of the image of scattered light are given in table below.

On the basis of the diagram above it may be assumed that the average values of areas of the bright regions of an image of scattered light for hard-to-cut materials did not differ in a substantial way. The highest values (from the range of 119,491–124,020 pixels) were visible in Zone I, where smears with the machined material were scarce or not present at all. In Zone II, in which there appeared medium size smears with the machined material, the values were slightly lower (from the range of 98,295–104,044 pixels). The values were lowest (from the range of 73,066–90,698 pixels) for Zone III, with many smears on the machined material. It may therefore be assumed that regardless of the type of hard-to-cut material, the differences in the values obtained were not significant. This means that the type of material had practically no influence on a major augmentation or reduction

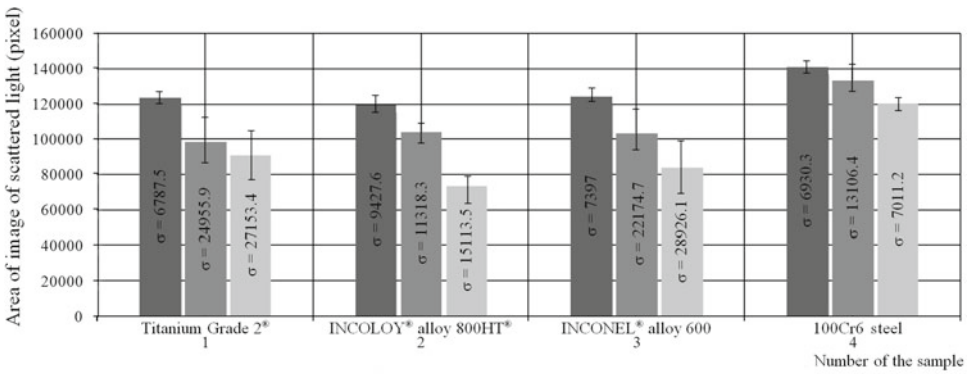

Zone I	123117	119491	124020	140818
Zone II	98295	104044	103592	133229
Zone III	90678	73066	83517	120235

Fig. 8 The results of computer image analysis—calculated average values of areas of the bright regions of an image of scattered light for the sample number (3 hard-to-cut materials + 1 reference material)

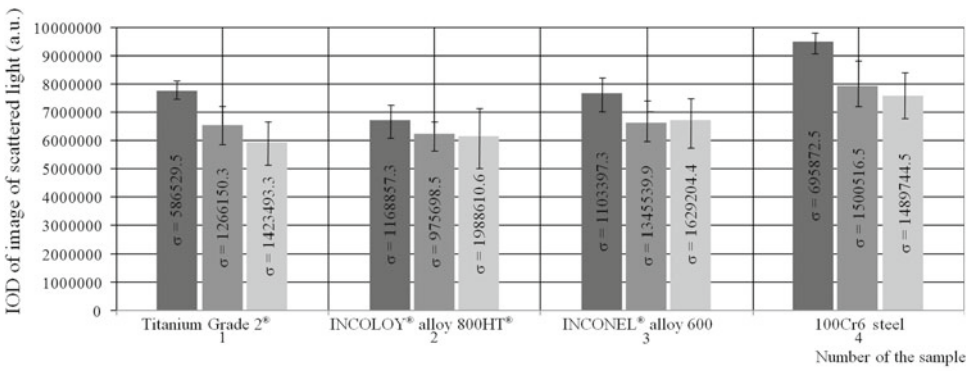

Zone I	7792891.2	6737321.1	7682368.8	9509755.0
Zone II	6556453.0	6250266.3	6662115.8	7957088.1
Zone III	5975215.4	6165967.8	6735670.5	7601145.1

Fig. 9 The results of computer image analysis—calculated average values of IOD of the bright regions of an image of scattered light for the sample number (3 hard-to-cut materials + 1 reference material)

Table 4 Percentage value decrease of calculated geometric and photometric parameters determined for hard-to-cut materials, compared with results of 100Cr6 steel

Material	Percentage value decrease (%)		
	Zone I	Zone II	Zone III
Area (of the bright regions of an image of scattered light) A_n			
Titanium Grade 2®	12.6	26.2	24.6
INCOLOY® alloy 800HT®	15.1	21.9	39.2
INCONEL® alloy 600	11.9	22.2	30.5
Integrated optical density (of the bright regions of an image of scattered light) I_Σ			
Titanium Grade 2®	18.1	29.2	19.2
INCOLOY® alloy 800HT®	17.6	21.5	16.3
INCONEL® alloy 600	21.4	18.9	11.4

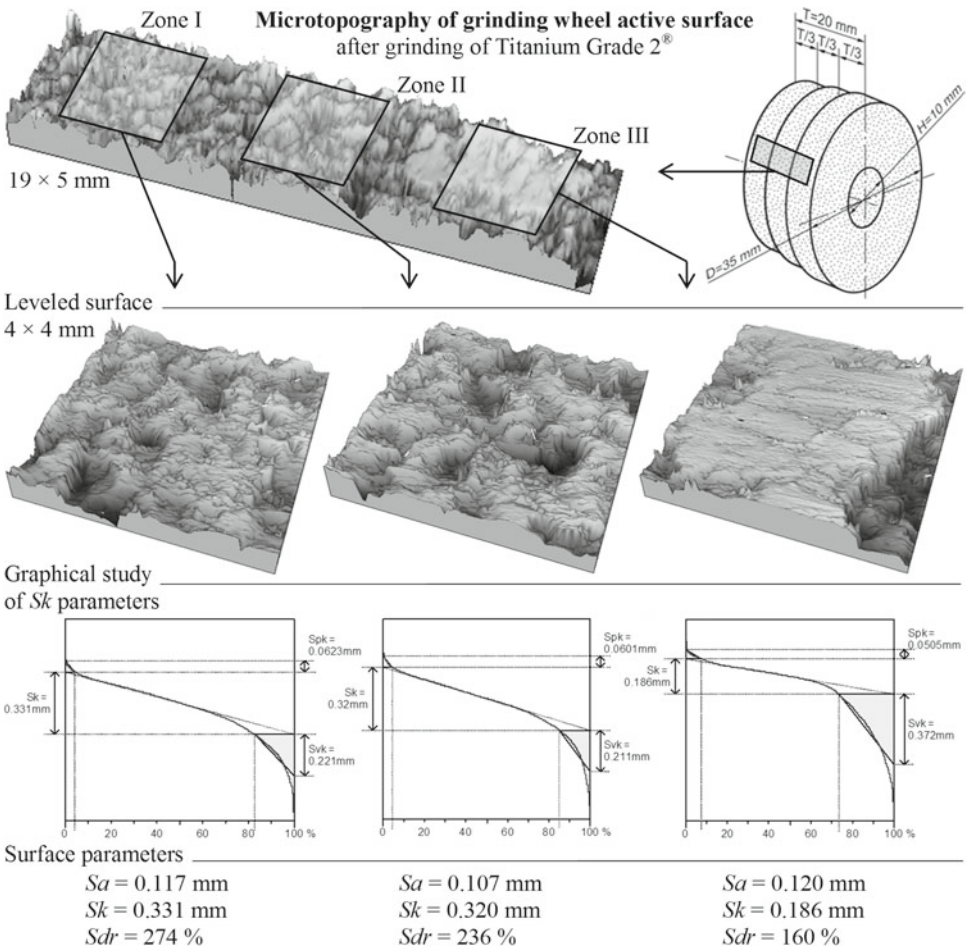

Fig. 10 The methodology of calculating the selected parameters of the GSS of the grinding wheel with shaped zones of various diameter, on the basis of a surface after grinding Titanium Grade 2®

of these values. Figure 8 also presents the average values of areas of the bright regions of an image of scattered light, acquired for the grinding wheel active surface after grinding the reference material, which, in this case, was 100Cr6 steel. The values were slightly higher because the grinding wheel was substantially less smeared. Its surface had practically no large and medium sized smears.

Figure 9 presents the results of computer image analysis—calculated average values of IOD of the bright regions of an images of scattered light for the sample number. In each column of the graphs, the values of standard deviation σ are also indicated. Additionally, the average values of IOD of the bright regions of an images of scattered light are given in the table below.

The averaged values of IOD of the bright regions of an image of scattered light gave similar results as the aforementioned graph presented in Fig. 8. Here, too, the levels of different average values of IOD of the bright regions of an image of scattered light, for three hard-to-cut materials, were similar. Moreover, the average values of IOD of the

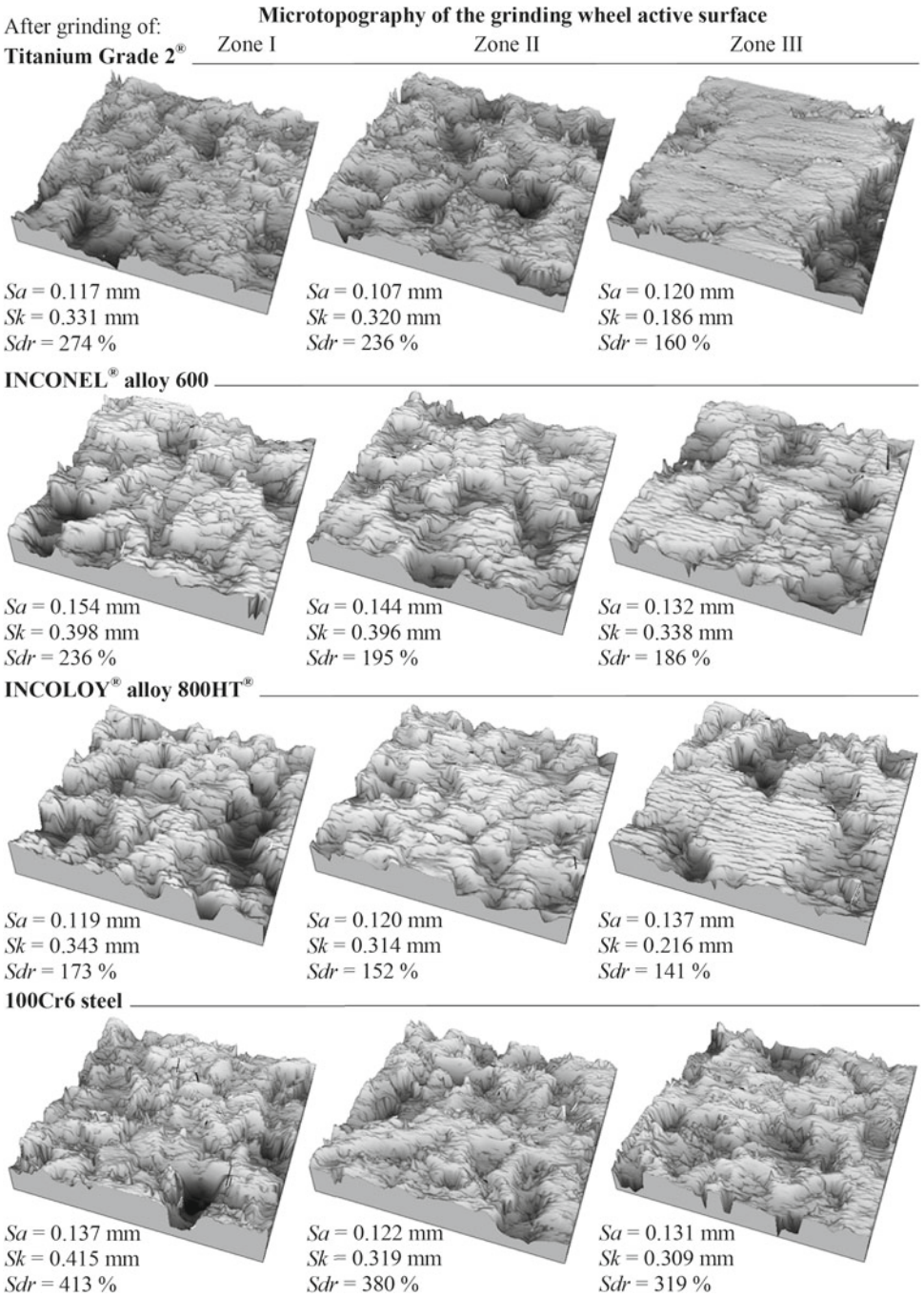

Fig. 11 Microtopographies and calculated selected parameters of GSS of the different zones of the grinding wheel active surface, with shaped zones of various diameter

bright regions of an image of scattered light for the reference material were higher, just as in the case of the average area values in Fig. 8. A certain correlation may then be observed between these two parameters of key importance for this analysis, which can only be an evidence of the fact that they were chosen appropriately.

While analyzing the graphs above a certain tendency may be noticed in the shaping of the values of the parameters described, if one differentiates between the zones of the grinding wheel active surface after grinding the next hard-to-cut material. In every case the values tend to decrease in comparison with the values obtained for the reference material (100Cr6 steel). Relative reduction of the parameter values for different zones of the grinding wheel active surface in percentage terms, are presented in Table 4.

The decreasing values of the assessed parameters for different zones of the grinding wheel active surface and the next hard-to-cut material mean that the optical method used was characterized by high sensitivity. Laser scatterometry is a method sensitive enough to allow for detection of grinding wheel smears of even a relatively small area. Among its

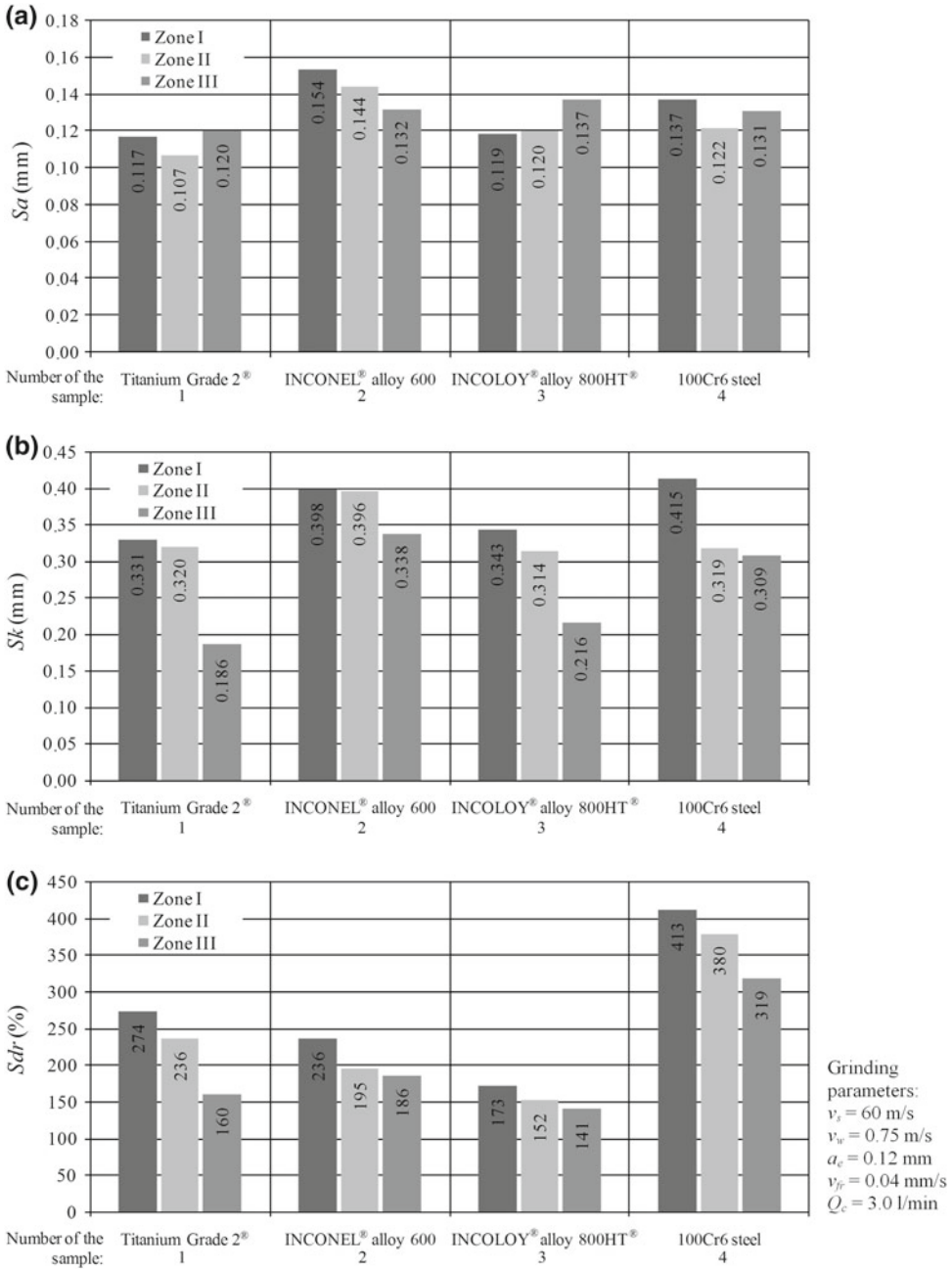

Fig. 12 Listing of the changes in values of the GSS parameters for 3 zones of the grinding wheel active surface after grinding Titanium Grade 2®, INCONEL® alloy 600, INCOLOY® alloy 800HT® and 100Cr6 steel: **a** arithmetic mean height *Sa*, **b** kernel roughness depth *Sk*, **c** developed interfacial area ratio *Sdr*

other advantages are: non-contact measurement, short time of assessment, a high degree of precision, and relatively simple measurement apparatus. An additional argument for choosing this method is the possibility of supporting it with the image processing and analysis techniques. This increases it's potential future applications, especially regarding the processing, analysis and visualization of the measuring data in the form of acquired static digital images. The method described can be an alternative to the other methods used in grinding tools' diagnostics.

Using the optical profilometry described earlier in Sect. 3, measurements were made of some surfaces of the grinding wheel active surface with visible smears. The results of these measurements were then analyzed using the TalyMap Universal 3.1.0 software.

Table 3 describes the characteristics of calculated selected parameters of the GSS chosen for the analysis of the measured microtopographies. First, a measurement was taken of the area, being a fragment of the grinding wheel active surface (size 19 × 5 mm), and then it was divided and leveled into the areas of 4 × 4 mm, corresponding to the 3 different working zones. On the basis of the topographies thus prepared, surface parameters were then calculated. The methodology of proceeding and calculating selected parameters of the GSS of the

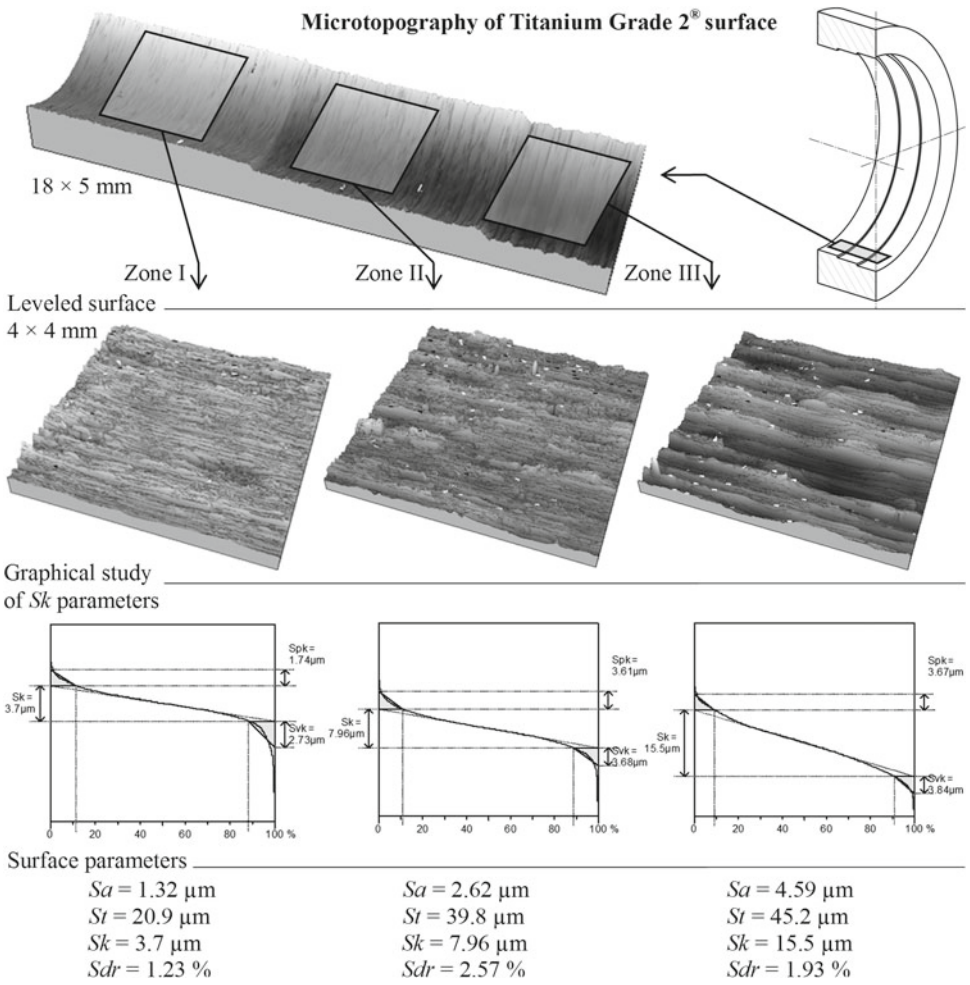

Fig. 13 The methodology of calculating selected GSS parameters of workpiece surface ground using a grinding wheel with zones of various diameter, on the basis of the surface of Titanium Grade 2®

grinding wheel are shown in Fig. 10. Additionally there was shown an example of surface microtopographies for three different working zones of the grinding wheel after grinding Titanium Grade 2®.

In Fig. 11 were shown the microgeometric views of different areas of the grinding wheel active surface, together with the values of the GSS parameters, calculated after machining four machined materials considered in the investigation.

The values of an arithmetic mean height *Sa* in different zones of the grinding wheel active surface are presented as a graph in Fig. 12a. The values did not vary to any great extent and their dispersion was never higher than 30 %. The calculated values of this parameter are mainly the result of the open structure of the grinding wheels used in the experimental investigations.

If one compares the values of kernel roughness depth *Sk* for different zones of the grinding wheel active surface (Fig. 12b), the influence of the smears upon the active surface, in different zones of the grinding wheel, is clearly visible. As the time and depth of grinding increases, so does the phenomenon of microsmearing of the abrasive grains and smearing of the intergranular free spaces, which reflect the changes in the value of kernel roughness depth *Sk*. The value of this parameter may also be influenced by the dullness of the abrasive grain's vertex. A substantial number of smears in Zone III of the measured grinding wheel's fragment are visible after grinding Titanium Grade 2® and INCOLOY® alloy 800HT®. In both the cases the value of the parameter for Zone III was c.a. 40 % lower in comparison to the value in Zone I.

The level of the *Sdr* parameter's values, which describes the degree of surface development for different functional zones of the grinding wheel active surface, has been much lower for the surface of the grinding wheel after grinding hard-to-cut materials, in comparison to the results after grinding 100Cr6 steel (Fig. 12c). This is further evidence of the parameter's sensitivity to smears upon the grinding wheel active surface, as (according to visual analysis of the grinding wheels under investigation) they did not appear in the case of grinding 100Cr6 steel.

The highest difference between Zone I (*Sdr* = 274 %) and III (*Sdr* = 160 %), namely that of 70 %, was observed in the case of the grinding wheel active surface after grinding Titanium Grade 2®. Such a great change in the value was

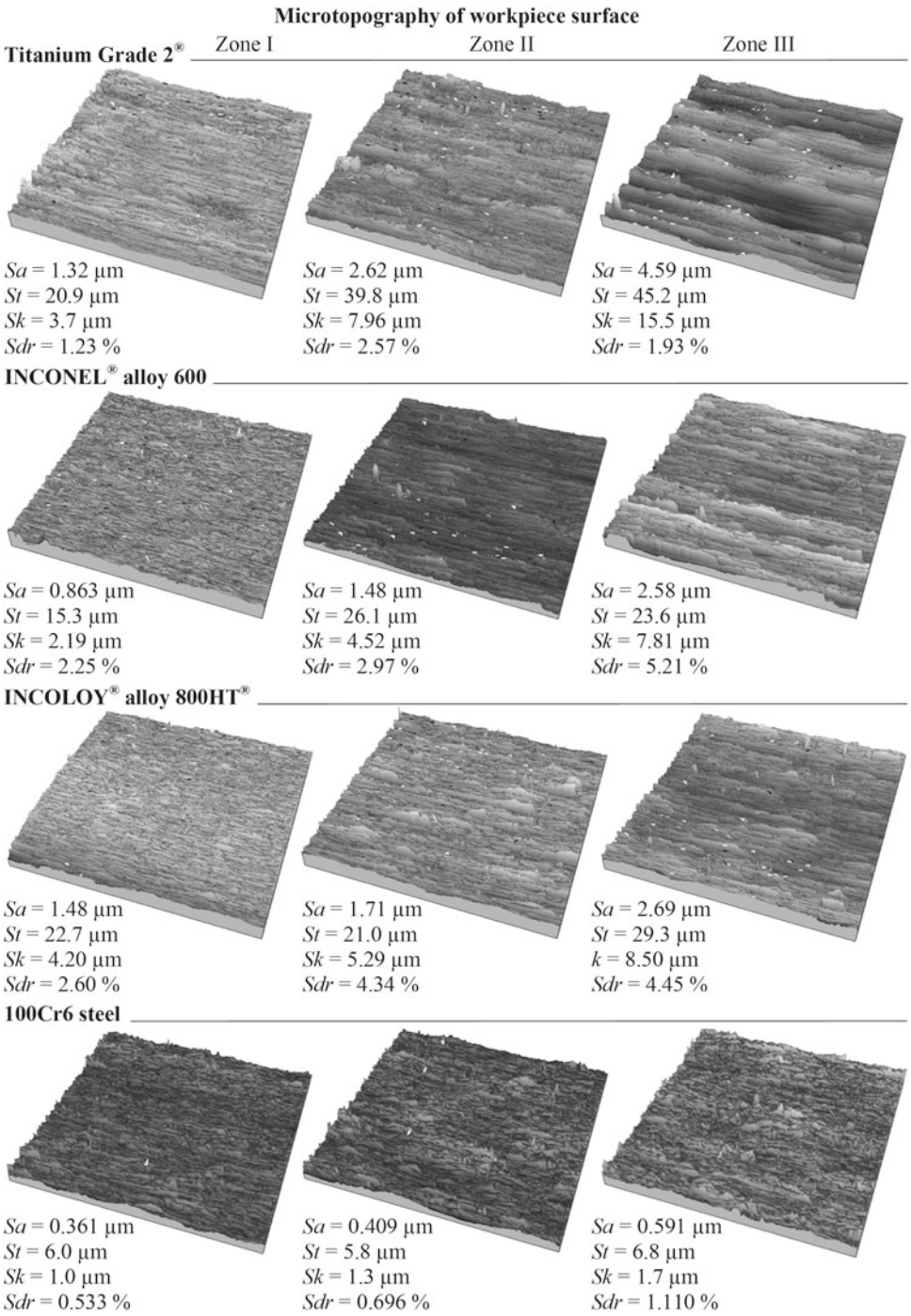

Fig. 14 Microtopographies of individual surfaces of the workpiece and calculated values of selected GSS parameters after grinding using a grinding wheel with zones of various diameter

caused by extensive smearing of intergranular free spaces, with smears clearly visible in the obtained microtopographies (Fig. 11) and in the micrograph visible in Fig. 3. For the remaining machined materials, the values of the *Sdr* parameter for each zone didn't show differences higher than that of 30 %.

In the case of the microtopography of the surface elements, analogical proceedings were used after grinding in order to calculate the parameters describing the GSS in three different machining zones (Fig. 13). The only difference was the fact that in the beginning a microtopography of 18 × 5 mm was measured for the machined surfaces.

Figure 14 shows the microtopographical images of different zones of the workpiece surfaces, and the calculated values of selected parameters of the surface's geometrical structure, taken int account during the investigation of the materials.

In the case of most of the investigated materials there is a visible increase in the value of the GSS parameters for subsequent grinding zones (Fig. 15). It means that as the grinding depth increases, so do the cross-sections of the layers ground

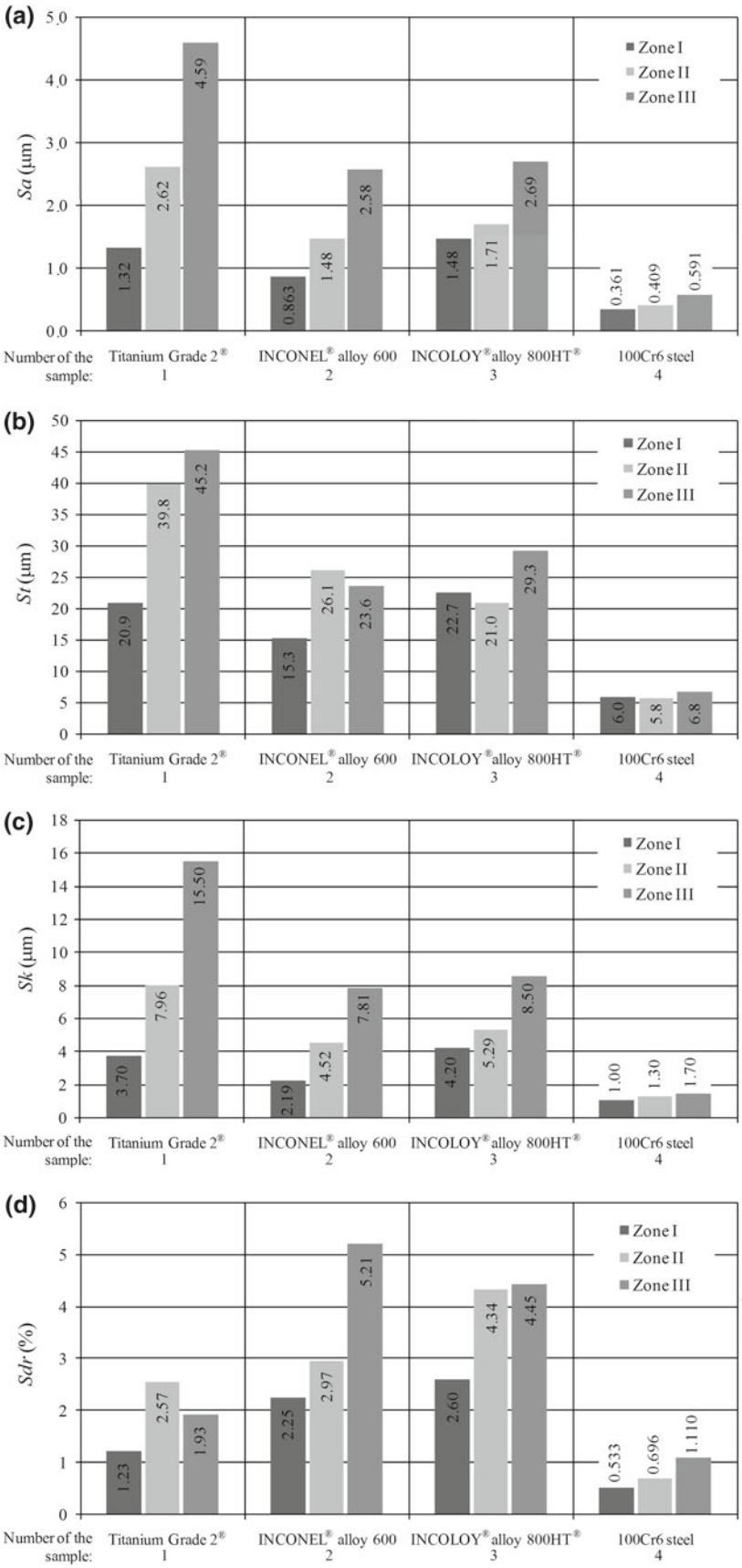

Fig. 15 The changes in calculated selected GSS parameters for three zones of the surface of Titanium Grade 2®, INCONEL® alloy 600, INCOLOY® alloy 800HT® and 100Cr6 steel: **a** arithmetic mean height *Sa*, **b** total height of the surface *St*, **c** kernel roughness depth *Sk*, **d** developed interfacial area ratio *Sdr*

with single abrasive grains which shape the surface of higher roughness.

The values of selected parameters calculated for the surface of Titanium Grade 2® after grinding with machining zone III of the grinding wheel active surface are characteristically high. This results from the fact that, in the case of titanium, changing the depth and time of grinding had a much higher influence on the structure of the machined surface. This was probably influenced by the increasing temperature in the contact zone between the grinding wheel and the machined material.

The highest roughness of the machined surface of titanium in Zone III did not only become apparent in the case of the *Sdr* value of surface development (Fig. 15d). The highest *Sdr* values were calculated for the surface of Zone III of INCONEL® alloy 600 and Zones II and III of INCOLOY® alloy 800HT®.

The calculated values of selected GSS parameters of the machined element clearly indicates the significant influence of the grinding parameters, here together with the condition of grinding wheel active surface, and especially the degree to which smearing is present.

The data presented here clearly indicate a correlation in the calculated values of parameters describing the acquired images of scattered light and the parameters describing the geometrical structure of both the grinding wheel active surface and the surface of the machined elements.

Parameter analysis of the results of the measurement techniques adopted here, together with visual analysis of the micrographs have shown a higher degree of smearing upon the grinding tools active surface after grinding the hard-to-cut materials. Among the samples chosen for the investigation, those which showed the largest areas of smears were made of Titanium Grade 2®—a fact additionally supported by the presented measurement results.

5 Conclusion

The results obtained from these investigations allow for a statement that the methods proposed in the article could be used for the purposes of assessing the condition of the grinding wheel active surface. This pertains to both its structure and the nonspecific elements which appeared on its surface as a result of different harmful phenomena accompanying the machining process. One of these nonspecific elements, described in this paper, is smearing. The intensive growth of smears leads to a decrease of the machining capacity of the grinding wheel, a reduction in its efficiency, increases in its grinding power and the participation of friction in the process. It also results in increasing the temperature in the contact zone between the grinding wheel and the workpiece, which intensifies the appearance of such grinding defects as grinding burns. In this context, proper diagnostics of grinding tools turns out to be a problem of relatively high importance. As the research results presented here have shown, the methods the authors used may be an interesting way of solving this problem. They may also be an alternative to the methods already in use. Laser scatterometry is characterized by high sensitivity, which allows for precise location and identification of smears. Supporting it with computer image processing and analysis techniques makes it possible to run an advanced image analysis in order to obtain more detailed information about the condition of the surface under investigation. The considerable usefulness of the methods used may allow for their future application in low-cost industrial, or laboratory, measuring apparatus with the characteristic improvements of non-contact measuring, short-time measurements and high accuracy.

Acknowledgments Part of this work was supported by the Polish Ministry of Science and Higher Education under Grant No. N503 214837. The authors would like to thank the anonymous reviewers for their helpful comments and suggestions, which greatly improved the manuscript. The authors would also like to thank all the employees of Koszalin University of Technology for their help and support in selected steps of experimental investigations: Mr. Andrzej Nowicki from Laboratory Team I for preparing grinding wheels for tests, Mr. Adam Szpakowicz, MSc, BSc, from Unconventional HydroJetting Technology Center, for the optical measurements of surface microtopography of tested grinding wheels, Mr. Krzysztof Maciejewski from Laboratory of Metrology And Measurement Systems for the stylus measurements of surface microtopography of workpieces as well as Mr. Ryszard Gritzman from Central Laboratory of Institute of Mechatronics, Nanotechnology and Vacuum Technique for acquisition of SEM micrographs.

References

1. Rowe, W.B.: Principles of Modern Grinding Technology. William Andrew Applied Science Publishers, Burligton (2009)
2. Webster J.; Tricard, M.: Innovations in abrasive products for precision grinding. Ann. CIRP **53**(2), 597–617 (2004)
3. Slowiński, B.; Nadolny, K.: Effective manufacturing method for automated inside diameter grinding. J. Adv. Mech. Des. Syst. Manuf. **1**(4), 472–480 (2007)
4. Nadolny, K.; Plichta, J.: Possibilities of development in the single-pass internal cylindrical grinding. In: Proceedings of the 19th International Conference on Systems Engineering (ICSENG), pp. 230–235. Las Vegas, USA (2008)
5. Nadolny, K.; Slowiński, B.: Potential for increasing the effectiveness of automated production systems due to application of single-pass grinding. Adv. Manuf. Sci. Technol. **34**(2), 19–30 (2010)
6. Xu, X.; Yu, Y.; Huang, H.: Mechanisms of abrasive wear in the grinding of titanium (TC4) and nickel (K417) alloys. Wear **255**, 1421–1426 (2003)
7. Tso, P.-L.: Study on the grinding of Inconel 718. J. Mater. Process. Technol. **55**, 421–426 (1995)

8. Ezugwu, E.O.: Key improvements in the machining of difficult-to-cut aerospace superalloys. Int. J. Mach. Tools Manuf. **45**, 1353–1367 (2005)
9. Teicher, U.; Ghosh, A.; Chattopadhyay, A.B.; Künanz, K.: On the grindability of titanium alloy by brazed type monolayered superabrasive grinding wheels. Int. J. Mach. Tools Manuf. **46**, 620–622 (2006)
10. Bentley, S.A.; Goh, N.P.; Aspinwall, D.K.: Reciprocating surface grinding of a gamma titanium aluminide intermetallic alloy. J. Mater. Process. Technol. **118**, 22–28 (2001)
11. Jackson, M.J.: Microscale wear of vitrified abrasive materials. J. Mater. Sci. **39**, 2131–2143 (2004)
12. Stover, J.C.: Optical Scattering: Measurement and Analysis. McGraw-Hill, Inc., New York (1990)
13. Ogilvy, J.A.: Theory of Wave Scattering from Random Rough Surfaces. Adam Hilger, Bristol, Philadelphia, New York (1991)
14. Iaquinta, J.; Fouilloux, A.: Modeling of light scattering by rough surfaces with relevance to pavements monitoring sensors. Opt. Lasers Eng. **41**, 687–702 (2004)
15. Tay, C.J.; Wang, S.H.; Quan, C.; Ng, C.K.: Surface roughness measurements of semiconductor wafers using a modified total integrated scattering model. Optik **113**, 317–321 (2002)
16. Zhang, Z.M.; Zhu, Q.Z.: Correlation of angle-resolved light scattering with the microfacet orientation of rough silicon surfaces. Opt. Eng. **44**(7), 073601 (2005)
17. Petit, J.; Boher, P.; Leroux, T.; Barritault, P.; Hazart J.; Chaton, P.: Improved CD and overlay metrology using an optical Fourier transform instrument. Proc. SPIE **5752**, 420–428 (2005)
18. Baumgart, J.W.; Truckenbrodt, H.: Scatterometry of honed surfaces. Opt. Eng. **37**(5) 1435–1441 (1998)
19. Rao, B.C.; Raj, B.: Study of engineering surfaces using laser-scattering techniques. Sādhanā. **28**(34), 739–761 (2003)
20. Łukianowicz, Cz.: Principles of Surface Roughness Measurements by Light Scattering Method. Technical University of Koszalin, Koszalin (in Polish) (2001)
21. Dupareé, A.: Light scattering techniques for the inspection of microcomponents and microstructures. In: Osten, W. (ed.) Optical Inspection of Microsystems. CRC Press, New York (2007)
22. Tay, C.J.; Quan, C.: A parametric study on surface roughness evaluation of semiconductor wafers by laser scattering. Optik **114**(1), 1–6 (2003)
23. Heintze, M.; Schmid, P.E.; Levy, F.; Weis P.; Guy, R.: Characterization of polycrystalline and amorphous silicon films by angle-resolved light scattering. J. Phys. D Appl. Phys. **26**(2), 271–280 (1993)
24. Ando, M.; Negishi, M.; Takimoto, M.; Deguchi, A.; Nakamura, N.: Supersmooth polishing on aspherical surfaces. Nanotechnology **6**, 111–120 (1995)
25. Chiou, Y.-C. Lee, R.-T.; Yau, C.-L.: A novel method of composite electroplating on lap in lapping process. Int. J. Mach. Tools Manuf. **47**, 361–367 (2007)
26. Kapłonek, W.; Łukianowicz, Cz.: Laser scatterometry used for assessment of microfinished shafts. In: Adamczak, S.; Stępień, K. (eds.) Proceedings of the IV. International Congress on Precision Machining ICPM 2007, pp. 291–296. Publications Kielce University of Technology, Kielce (2007)
27. Kapłonek, W.; Łukianowicz, Cz.: Laser scatterometry and image analysis used for the assessment of surface roughness of microfinished cylindrical elements made of plastics. Meas. Autom. Monit. **56**(4), 330–333 (2010)
28. Kapłonek W.; Łukianowicz, Cz.: Assessment of surface roughness in movement by image stacking. In: Pawlus, P.; Blunt, L.; Rosen, B-G.; Thomas, T.; Wieczorowski, M.; Zahouani, H. (eds.) Proceedings of the 12th International Conference on Metrology and Properties of Engineering Surfaces, pp. 295–299. Publications Rzeszów University of Technology, Rzeszów (2009)
29. Stout, K.J.; et al.: The Development of Methods for the Characterization of Roughness in Three Dimensions. Publication No. EUR 15178 EN (Final Report) BCR, European Community, Brussels (1993)